

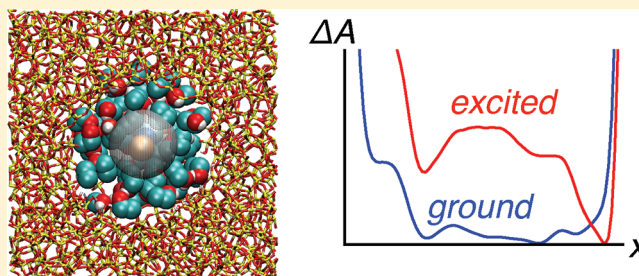
# Solvation and Spectra of a Charge Transfer Solute in Ethanol Confined within Nanoscale Silica Pores

Anthony A. Vartia and Ward H. Thompson\*

Department of Chemistry, University of Kansas, Lawrence, Kansas 66045, United States

**S** Supporting Information

**ABSTRACT:** The free energy and electronic fluorescence spectra of a model solute solvated by ethanol in a nanoscale silica pore are examined as a function of the solute position, with the aim of improving our understanding of solvation in nanoconfined environments. The results indicate that the position distribution of the solute depends on its dipole moment as well as on the surface interactions of the silica pore, i.e., hydrophilic or hydrophobic (uncharged). Further, the solute fluorescence spectrum is a function of the solute position in the hydrophilic pore, but is independent of position in the hydrophobic pore. The origins of these results are investigated, including by decomposition of the free energy as a function of solute position into the contributing interactions. The implications for time-dependent fluorescence (TDF) experiments, used commonly to probe solvation dynamics in nanoconfined solvent systems, are considered. The possible role of chromophore diffusion in TDF measurements, and chemistry in nanoconfined liquids more broadly, is given particular emphasis.



## 1. INTRODUCTION

Confinement of liquids on nanometer length scales dramatically alters their properties, including diffusion,<sup>1–4</sup> reorientation,<sup>4–32</sup> conformational equilibria,<sup>33–35</sup> reaction kinetics,<sup>36–52</sup> and solvation dynamics.<sup>52–79</sup> The impact of nanoconfinement on such a diverse set of chemistries naturally translates to a broad range of applications. Thus, nanoconfining materials such as zeolites, reverse micelles, and mesoporous silicates have received significant attention for their potential as drug delivery vehicles, chemical sensors, and catalysts, among others. The rational design of these materials for applications requires connecting the modified properties listed above to the confining framework characteristics.

A key element in this regard is understanding how nanoconfinement affects solvation. Processes involving charge transfer in polar solvents, a broad and important group, are typically coupled strongly to collective solvent motions, the same motions probed in solvation dynamics measurements such as time-dependent fluorescence (TDF) experiments. In a typical TDF measurement, dye molecules in the electronic ground state are promoted to an electronic excited state at a time defined as  $t = 0$ . Within the Franck–Condon approximation, the solvent is in a nonequilibrium configuration with respect to the new charge distribution of the solute. The solvent molecules thus reorganize to stabilize the solute until the solvent is in equilibrium with the excited-state solute. The solute fluorescence energy then depends on the time  $t$  after excitation, as a result of the solvent rearrangement. The change in fluorescence energy as a function of time reports on these solvent dynamics. In general, the normalized TDF signal,  $S(t)$ ,

$$S(t) = \frac{\langle \Delta E_{\text{fl}}(t) \rangle - \langle \Delta E_{\text{fl}}(\infty) \rangle}{\langle \Delta E_{\text{fl}}(0) \rangle - \langle \Delta E_{\text{fl}}(\infty) \rangle} \quad (1)$$

is fit with a single- or multiexponential function. Often the time constant in each exponential function is related to a particular solvent motion, e.g., inertial, librational, or reorientational dynamics.

In nanoconfined systems, TDF experiments generally find a solvation response that is considerably slowed relative to that of the bulk liquid, as discussed in detail in a recent review.<sup>52</sup> This can occur in two ways. In the first, the normalized dynamic Stokes shift,  $S(t)$ , in the confined solvent can be fit to the same multiexponential expression as in the bulk liquid, but with time constants that are significantly longer. In the second,  $S(t)$  in the confined solvent can only be fit by invoking additional exponential time scales beyond those required for the bulk solvent.<sup>68,69,80–91</sup> These additional time scales are long compared to those found in the bulk and suggest that confinement leads to emergent dynamics with no bulk counterpart. Multiple models have been proposed to explain these new time scales. For example, these emergent time scales have been attributed to subpopulations of solvent with different dynamics in the commonly invoked two-state, or core–shell, model.<sup>7,9,16,17,21,24,27,30,32,33,35,92–95</sup> The exchange of solvent molecules adjacent to the solute has been implicated in another proposed mechanism.<sup>71,74</sup> We have previously suggested that solute diffusion after excitation could lead to additional time

**Received:** November 8, 2011

**Revised:** April 6, 2012

**Published:** April 6, 2012

scales in the TDF signal.<sup>75,76</sup> There is as yet no definitive test of the different proposed mechanisms, and thus, our molecular-level understanding of the information content in the TDF signal of nanoconfined systems is incomplete, making the interpretation of such TDF spectra difficult.

In this paper, we further examine the possible role of solute diffusion in the emergent time scales observed in TDF measurements in nanoconfined solvents. It is important to note that while the diffusion constant itself may affect the quantitative details,<sup>78</sup> whether or not solute diffusion is manifested in the TDF signal is determined by how the free energy depends on the solute position. Previous work in our group<sup>75,76</sup> has shown that small model solutes in solvents confined within nanoscale cavities do exhibit solute diffusion after excitation that gives rise to an additional time scale in the TDF signal, compared to the bulk solvent. The simplicity of those models allows an examination of the underlying causes of this behavior, e.g., entropic and energetic contributions,<sup>96</sup> which suggest the phenomenon is general. However, it is less clear how the solute diffusion can be modified (and to what degree it would be observable) in a TDF experiment. Specifically, the effects of solute size and charge distributions as well as confining framework structure and interactions are not clear. The variety of different behaviors observed in TDF measurements on confined solvents suggests that the mechanism(s) responsible for the longer time scale dynamics may vary with the system.

In order for solute diffusion after excitation to explain the emergent time scales in TDF experiments, the system must satisfy three requirements:<sup>52</sup> (1) The position of the solute (dye) within the confining framework must be state-dependent, as previously observed in model confining frameworks.<sup>75,76,97</sup> (2) The dye fluorescence spectrum must be a function of position within the confining framework with shifts that are sufficiently large to be measurable.<sup>75,76,97</sup> (3) Upon excitation, the dye diffusion and associated spectral shifts must occur on experimentally accessible time scales. In the present work, requirements 1 and 2 outlined above are addressed using equilibrium molecular dynamics (MD) simulations of a simple dye model dissolved in ethanol and confined in a silica pore. However, it is important to note that the dependence of the solute position distribution, which is at the heart of requirement 1, has implications for chemistry in nanoconfined solvents far beyond TDF measurements.

The present work is aimed at addressing these issues related to state-dependent solute positions and the relevance to TDF measurements. Specifically, the focus is on uncovering the fundamental thermodynamics that may drive solute diffusion after excitation. Thus, the free energy curves that ultimately govern the diffusion in such nanoconfined systems are examined. The present simulations are motivated, in part, by TDF experiments by Baumann et al. on coumarin 153 within ethanol-containing silica pores of 2.5 and 5.0 nm diameter.<sup>65</sup> They found the decay of the TDF signal,  $S(t)$ , lengthened with decreasing pore size. Specifically, the two longest time scales in the decay (which was fitted to a triexponential) increased roughly 4- or 5-fold from the bulk liquid to the 2.5 nm pore. A qualitatively similar effect on  $S(t)$  upon confinement was also obtained by Kamijo et al. for a silica pore system and the same dye molecule.<sup>66</sup> However, they obtained significantly longer absolute decay times for both the bulk and confined solvents. The system investigated here is a large, model solute dissolved in ethanol confined within  $\sim 2.4$  nm diameter hydrophilic and

hydrophobic silica pores. This is an intermediate modeling approach to probe the relevant issues and complements simulations with realistic dye molecules.

The organization of the remainder of the paper is as follows. Simulation details, including descriptions of the solvent, solute, and confining silica pore, are outlined in section 2. In section 3, both the state-dependent biasing of solute position, obtained from thermodynamic integration, and the position-dependence of the solute fluorescence energy are demonstrated. In section 4, we offer our interpretations and insights, including a discussion of key factors that affect the solute position distribution and fluorescence energy: solvent layering and surface heterogeneity. Section 5 offers conclusions and outlines future directions.

## 2. SIMULATION DETAILS

**2.1. Model Systems.** To model dye molecules with ground- and excited-state charge distributions, solute models with dipole moments of 5, 10, and 15 D were constructed in the spirit of the Stockmayer liquid. The solute model consists of 3 sites, one each for a center of positive charge (P), a center of mass (COM), and a center of negative charge (N). These sites are collinear with the charges on opposite sides of the COM (1.6 Å away); the charges, listed in Table S1 of the Supporting Information, thus give dipole moments of 5, 10, and 15 D. A mass of 50 amu is assigned to each charged site. The dye molecule is spherical with a size determined by a single Lennard-Jones site located at the COM. The  $\sigma$  for the dye is chosen to approximately yield the same volume as the coumarin 153 dye.<sup>98</sup> The Lennard-Jones  $\epsilon$  parameter value is chosen to be roughly similar to those of the solvent alkyl and silanol oxygen sites.

Ethanol was represented by the OPLS model,<sup>99,100</sup> modified to include Lennard-Jones parameters for the ethanol hydrogen atom equivalent to those for the silanol groups. The inclusion of these parameters for the ethanol hydrogen shows no effect on the ethanol liquid structure, but it is important to avoid spurious effects associated with ethanol–silica interactions.

The effects of nanoconfinement were investigated using the silica pore model previously developed in our group.<sup>35,101,102</sup> The pore is roughly cylindrical with a radius of  $\sim 12$  Å. The silica surface presents 36 silanol groups and 6 geminal silanol groups to the pore interior. Potential parameters for the silica atoms are given in the Supporting Information. The same pore structure is rendered hydrophobic by setting all pore atom charges to zero.

**2.2. Molecular Dynamics.** Molecular dynamics simulations were performed on systems comprising the model dye molecule dissolved in ethanol as a bulk liquid and confined in the silica pores. All simulations used the DL POLY 2<sup>103</sup> software package and were run in the NVT ensemble with  $T = 298$  K using a Nosé-Hoover thermostat.<sup>104,105</sup> Long-range electrostatics were handled by the damped shifted force method.<sup>106–108</sup> Equilibration phases lasted 200 ps, followed by production runs of 2 ns (1 fs time step). Configurations were sampled every 100 fs unless noted otherwise. All uncertainties were calculated using the Student  $t$  test with a 95% confidence interval by dividing each trajectory into five blocks.<sup>109</sup> The error bars in the free energy curves represent the uncertainties in the free energy relative to the global minimum of the curve, i.e., the uncertainty in  $\Delta A(x) - \Delta A_{\min}$ .

A schematic representation of the confined system is shown in Figure 1. The confined systems were initiated by overlapping

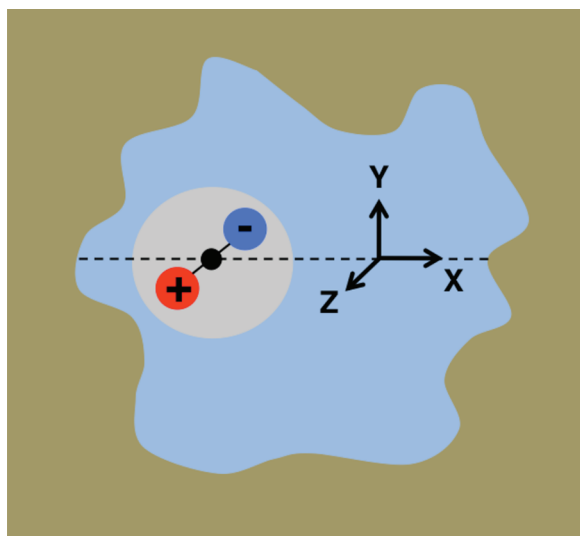


**Figure 1.** Schematic representation of the confined system (not to scale). A model solute (gray) dissolved in ethanol (light blue area) confined in a silica pore (tan area). Within the solute are positive charge (red, +) and negative charge (blue, -) sites. The solute center of mass (black) is used to hold the solute fixed at points along the  $x$  axis (dashed line).

a bulk simulation, with the solute frozen at the center of the cell, with the silica pore structure. Solvent molecules overlapping the silica pore were eliminated, leaving 121 ethanol molecules.<sup>110</sup>

**2.3. Calculations.** Free energy profiles were calculated using thermodynamic integration. Each free energy curve,  $\Delta A(x)$ , was calculated along a single coordinate within the pore, arbitrarily chosen as  $x$ . The potential on the solute COM site was calculated according to

$$U = \sum_{i=1}^{N_{\text{cut}}} \left\{ 4e \left[ \left( \frac{\sigma}{r_{i\text{COM}}} \right)^{12} - \left( \frac{\sigma}{r_{i\text{COM}}} \right)^6 \right] + \sum_{\alpha=N}^P \left\{ \frac{q_i q_{\alpha}}{4\pi\epsilon_0 r_{i\alpha}} \right\} \right\} \quad (2)$$

Here,  $i$  labels the solvent and pore sites,  $\alpha$  indexes the charged solute sites (N, P), and  $r_{i\text{COM}} = |\underline{r}_i - \underline{r}_{\text{COM}}|$  and  $r_{i\alpha} = |\underline{r}_i - \underline{r}_{\alpha}|$  are the distances between site  $i$  and the solute sites. The summation upper bound,  $N_{\text{cut}}$  is the number of sites for

which  $r_{i\text{COM}} < r_{\text{cut}}$  or  $r_{i\alpha} < r_{\text{cut}}$ , where  $r_{\text{cut}} = 15 \text{ \AA}$ . The total forces acting on the COM site of the dye along a Cartesian coordinate  $x$  were calculated from the potential according to eq 3:

$$F_x = -\nabla_r U \cdot \frac{\partial r}{\partial x} \hat{x} \quad (3)$$

where  $x$  and  $r$  here, and in the following, refer to the COM position. The forces were also decomposed into Coulombic and Lennard-Jones contributions from both the solvent and pore to permit calculation of the corresponding contributions to the total free energy profile. Integration of the average forces yields the Helmholtz free energy

$$\Delta A(x) \equiv A(x) - A(x_0) = - \int_{x_0}^x \langle F_{x'} \rangle dx' \quad (4)$$

To calculate  $\langle F_{x'} \rangle$ , the dye COM site was frozen at a specified  $x'$ , while the P and N charge sites of the solute were allowed to rotate. To investigate different pore interfaces, multiple, evenly spaced “cuts” through the pore were made by setting  $y = 0 \text{ \AA}$  and  $z = -10, 0$ , or  $+10 \text{ \AA}$ . For each cut through the pore, a different  $x_0$  was chosen to reflect strong repulsion of the solute by the pore surface, and the set of free energy calculations associated with that cut used the same  $x_0$  position. Along each cut, a series of simulations were carried out for a grid of dye molecule positions spaced by  $\Delta x = 0.2 \text{ \AA}$ . For each solute COM position,  $x$ , a full equilibration was performed, followed by a data collection stage.

From the resulting free energy profiles, the position probability distributions of the solute COM site within the pore were calculated according to the Boltzmann distribution.

$$P(x) = \frac{e^{-\beta \Delta A(x)}}{\int e^{-\beta \Delta A(x')} dx'} \quad (5)$$

To investigate the possibility that electronic spectra depend upon the position of the solute within the pore, individual spectra were calculated for each solute COM  $x$  position according to

$$I_{\text{abs}}(\Delta E; x) = \langle \delta[E_{\text{ex}}(\mathbf{Q}) - E_{\text{gr}}(\mathbf{Q}) - \Delta E] \rangle_{\text{gr},x} \quad (6)$$

$$I_{\text{fl}}(\Delta E; x) = \langle \delta[E_{\text{ex}}(\mathbf{Q}) - E_{\text{gr}}(\mathbf{Q}) - \Delta E] \rangle_{\text{ex},x} \quad (7)$$

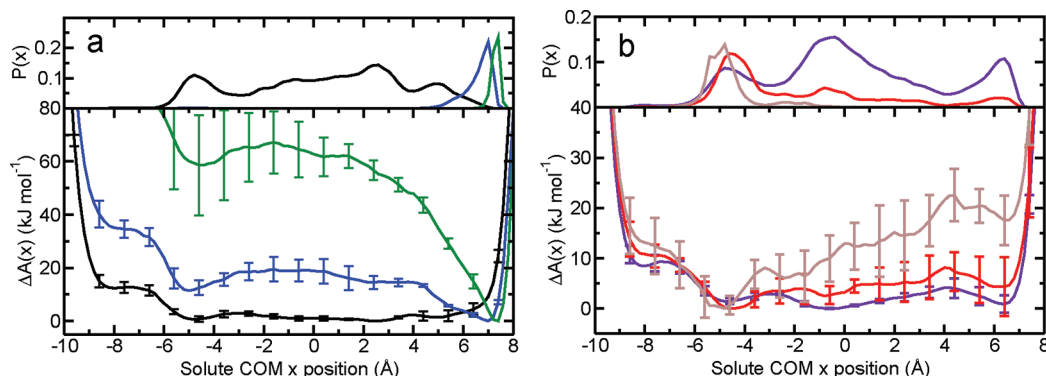


**Figure 2.** Free energy profiles,  $\Delta A(x)$ , and probability distributions,  $P(x)$ , in the hydrophilic pore (a) along  $z = 0$  for 5 D (black), 10 D (blue), and 15 D (green) solutes are shown;  $P(x)$  is scaled by 5 and  $1/2$  for 5 and 15 D, respectively. The corresponding information for the hydrophobic pore (b) for 5 D (purple), 10 D (red), 15 D (brown) is also provided;  $P(x)$  is scaled by 5 and 2 for 5 and 10 D, respectively. The error bars indicate uncertainties of the free energy change from the global minimum (which is set to zero separately for each curve).



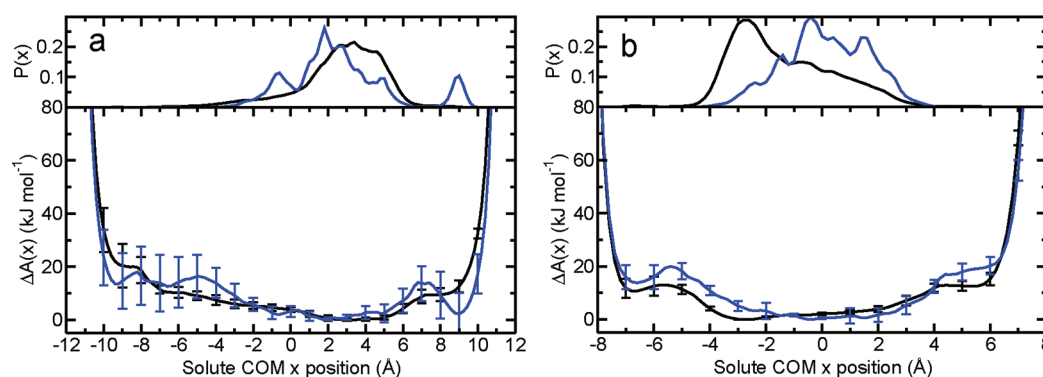


**Figure 3.** Same as Figure 2, but results are shown for the hydrophilic pore along cuts at (a)  $z = +10$  Å and (b)  $z = -10$  Å for 5 D (black) and 10 D (blue) solutes. In all cases,  $P(x)$  is scaled by a factor of 5.

The subscripted averages,  $\langle \cdot \rangle_{\text{gr},x}$  and  $\langle \cdot \rangle_{\text{ex},x}$  refer to averaging over pore and solvent configurations,  $\mathbf{Q}$ , that have been equilibrated to ground and excited state solutes, respectively, with the solute COM at position  $x$ . For selected solute positions, sampling was enhanced such that the difference between excited- and ground-state Coulombic energies was calculated every 20 fs.

### 3. RESULTS

**3.1. Free Energy and Solute Position.** The model solutes with dipole moments of 5, 10, and 15 D were each dissolved in ethanol confined in a  $\sim 12$  Å radius silica pore. The free energy and probability distributions as a function of solute position were calculated for these systems according to eqs 4 and 5, respectively. The results for the  $z = 0$  Å cut are presented in Figure 2 for the hydrophilic pore and the corresponding hydrophobic pore (with pore charges set to zero). From the figure, it is clear that both the solute dipole as well as the nature of the confining framework profoundly impact the free energy profiles for the solute, and that these in turn influence the solute location within the silica pore.

By examination first of the hydrophilic pore cases shown in Figure 2a, it is clear that increasing the dipole moment of the solute has a dramatic effect on the overall free energy profile across the pore. The 5 D solute can be considered as a model of the ground state of a typical dye molecule. The free energy for the solute is mostly flat across the pore, with diffusive barriers of less than  $2k_{\text{B}}T$ . This is reflected in the correspondingly broad position probability distribution, which indicates that the majority of the pore diameter should be accessible to the 5 D solute. The exception to this occurs near the left-hand side of the pore ( $x < -6$  Å), where the free energy rises approximately  $12 \text{ kJ mol}^{-1}$  with a corresponding decay in probability. Specific features of the free energy profiles, such as the rise in free energy near the left side of the pore and the small undulations in the average free energy profile, are discussed in section 3.2 in the context of the decomposition of the free energy profiles.

The 10 and 15 D solutes represent models of excited-state dye molecules. Both exhibit free energy curves that are clearly different from that of the 5 D solute. These free energy profiles generally decrease from left to right, and the magnitude of this effect is related to the dipole moment of the solute. This correspondingly modifies the position probability distributions. The result is that these solutes do not sample the pore interior, but instead are localized near the pore surface (on the right-hand side,  $x > 4$  Å).

Turning to behavior in the hydrophobic (uncharged) silica pore shown in Figure 2b, the 5 D solute behaves similarly in hydrophobic and hydrophilic confinement. In both environments, the free energy profile for this solute is relatively flat, resulting in a homogeneous position probability distribution. Additionally, both systems show the same increase in free energy near the left-hand side of the pore, and the same small undulations in the free energy curves (though for neither case are these undulations resolvable within statistical uncertainty).

Increasing the solute dipole moment to 10 or 15 D within the hydrophobic pore also results in biased distributions, but the effect, the depth of the free energy minimum, is diminished relative to the hydrophilic pore. However, the trend that the magnitude of the dipole controls the degree of solute localization is preserved. Notably, the biasing of the solute position in the hydrophobic pore occurs toward the left-hand side of the pore, in contrast to the hydrophilic pore.

It is natural to ask if the features in Figure 2 are general or specific to the chosen cut ( $z = 0$  Å) across the pore. This is explored in Figure 3, which shows  $\Delta A(x)$  and  $P(x)$  for 5 and 10 D solutes in the hydrophilic pore for cuts along  $x$  at  $z = +10$  Å (a) and  $z = -10$  Å (b);  $y = 0$  Å for both cases. These cuts also exhibit relatively flat free energy curves for the 5 D solute with correspondingly delocalized position distributions. Moreover, in each case, changing the dipole moment leads to a different position distribution for the solute. In some cases (the right-hand sides of the pore cuts for  $z = 0$  and  $10$  Å) this is a consequence of stronger solute affinity for the pore surface with increasing solute dipole moment. That this is only true for certain locations on the pore surface is a demonstration of the effect of pore heterogeneity. In the remaining cases, the free energy for both the 5 and 10 D solutes rises as the solute approaches the pore surface. As discussed in section 4.3, this likely represents the cost of displacing ethanol solvent molecules at the surface.

Taken together, the three free energy curves for different paths across the pore find that (1) the 5 and 10 D solutes always have different position distributions, and (2) particular locations at the pore surface attract the 10 D (and 15 D) solute due to favorable pore–solute interactions (see section 3.2), an indication of the heterogeneity of the amorphous silica pores. The implications of these results are discussed in section 4.

**3.2. Free Energy Decomposition.** The variability in the solute position distributions for different cuts across the pore naturally raises the following question: What controls the overall shape of the free energy profiles? To answer this, the solute free energies were decomposed into solvent,  $\Delta A_{\text{solv}}(x)$ ,

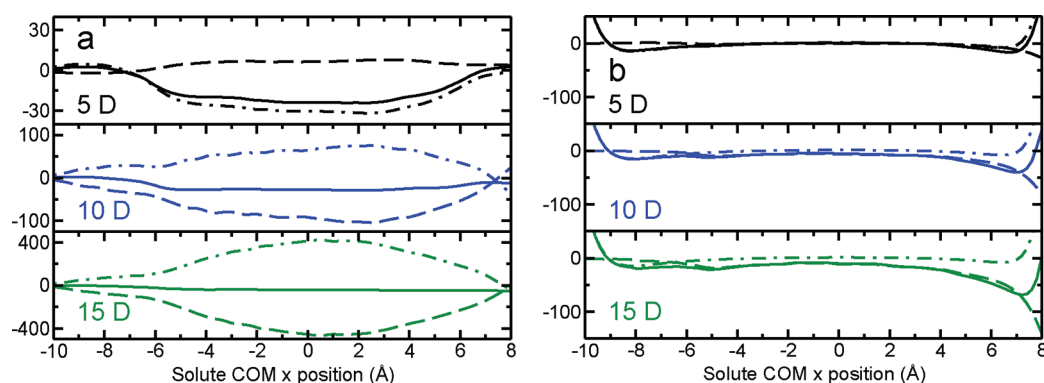


**Figure 4.** Free energy decompositions in the hydrophilic pore,  $z = 0$  Å cut, for (a) solute–solvent contributions to the free energy (in  $\text{kJ mol}^{-1}$ ),  $\Delta A_{\text{solv}}$  (—),  $\Delta A_{\text{solv,C}}$  (---), and  $\Delta A_{\text{solv,LJ}}$  (— · —), for 5 (top), 10 (middle), and 15 (bottom) D solutes, and (b) solute–pore contributions  $\Delta A_{\text{pore}}$  (—),  $\Delta A_{\text{pore,C}}$  (---), and  $\Delta A_{\text{pore,LJ}}$  (— · —). Note the changes in the free energy scale. In part b, the total and Lennard-Jones contributions have been shifted by  $400 \text{ kJ mol}^{-1}$  for plotting purposes.

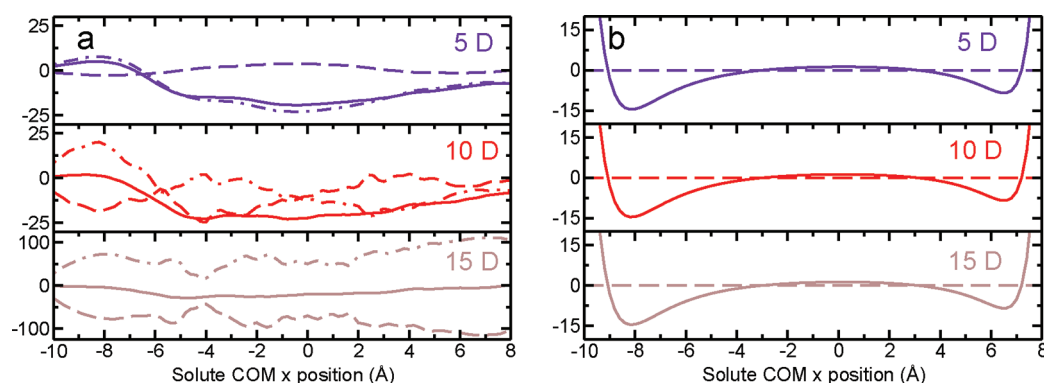


**Figure 5.** Same as Figure 4, but for the hydrophobic pore. Note that, for the solute–pore contributions to the free energy in part b, the total and Lennard-Jones contributions are equal.

and pore,  $\Delta A_{\text{pore}}(x)$ , contributions such that  $\Delta A(x) = \Delta A_{\text{solv}}(x) + \Delta A_{\text{pore}}(x)$ . These were further separated into Coulombic and Lennard-Jones components where  $\Delta A_{\text{solv}}(x) = \Delta A_{\text{solv,C}}(x) + \Delta A_{\text{solv,LJ}}(x)$  and  $\Delta A_{\text{pore}}(x) = \Delta A_{\text{pore,C}}(x) + \Delta A_{\text{pore,LJ}}(x)$ .

The free energy decompositions for hydrophilic pores along the cut  $z = 0$  Å, shown in Figure 4, are considered first. The contributions to the free energy from solute–solvent interactions ( $\Delta A_{\text{solv}}$ ,  $\Delta A_{\text{solv,C}}$ , and  $\Delta A_{\text{solv,LJ}}$ ) are presented in Figure 4a. For the 5 D solute in the hydrophilic pore, the Lennard-Jones interactions dictate the overall form of the free energy curve, and only relatively small additions come from Coulombic components. The result is a solvent contribution to the free energy that shows a shoulder on each side of the pore, indicating that  $\Delta A_{\text{solv}}(x)$  favors a solute in the pore interior. The physical picture is one in which the solute is better solvated by the solvent in pore locations where the solvent has greater access to the solute. Interestingly, for the 10 and 15 D solutes,  $\Delta A_{\text{solv,C}}(x)$  and  $\Delta A_{\text{solv,LJ}}(x)$  reverse sign compared to the 5 D solute case. Regardless, the two contributions nearly cancel so that the minimum in  $\Delta A_{\text{solv}}(x)$  for the 10 and 15 D solutes is located in the pore interior just as for the 5 D case. Notably, these observations also hold for the cuts along  $z = -10$  Å and  $z = +10$  Å (not shown).

The solute–pore contributions ( $\Delta A_{\text{pore}}$ ,  $\Delta A_{\text{pore,C}}$ , and  $\Delta A_{\text{pore,LJ}}$ ) in the hydrophilic pore along the  $z = 0$  Å cut are shown in Figure 4b. For all solutes,  $\Delta A_{\text{pore,LJ}}(x)$  is near zero in the pore interior, reaches a minimum near the pore wall, and then rises steeply as the solute presses against the pore surface.

On the other hand,  $\Delta A_{\text{pore,C}}(x)$  is also small in the interior, but becomes increasingly negative on the right-hand side ( $x > 0$ ) as the solute approaches the pore surface. Notably, increasing the solute dipole results in stronger Coulombic attraction to the pore wall. A similar pattern might be expected for the left-hand side of the pore as well, but this is absent, a reflection of the heterogeneity of the pore surface. The results for the  $z = +10$  Å cut are similar to the  $z = 0$  Å case, though with a less pronounced decrease in  $\Delta A_{\text{pore,C}}(x)$  near the pore surface. On the other hand, the Coulombic interactions with the pore surface are weak for  $z = -10$  Å, analogous to the left-hand side ( $x < 0$ ) for the  $z = 0$  Å case shown in Figure 4b.

It is clear from Figure 4 that the solute–pore interactions,  $\Delta A_{\text{pore}}(x)$ , control the overall shape of the free energy landscape, while solute–solvent interactions,  $\Delta A_{\text{solv}}(x)$ , contribute the finer structure, the shoulders and the small undulations in the curves. This is a general phenomenon also seen in the cuts along  $z = -10$  and  $z = +10$  Å. The free energy decompositions support the notion that pore surface properties dictate the solute position distribution: the surface heterogeneity is thus a key factor in solute behavior.

The analogous free energy decompositions into solvent and pore contributions for the solute series in the hydrophobic pore are shown in Figure 5. It is clear by comparing Figures 4a and 5a that the surface interactions of the confining framework significantly affect the strength of the solute–solvent contributions,  $\Delta A_{\text{solv}}$ ; note the differences in free energy scale. Despite this, the solute–solvent interactions exhibit a

near-cancellation of  $\Delta A_{\text{solv,C}}$  and  $\Delta A_{\text{solv,LJ}}$  resulting in the same qualitative behavior in the free energy curves.

The solute–pore contributions in the hydrophobic pore are plotted in Figure 5b. Because the pore charges have been set to zero in this case,  $\Delta A_{\text{pore}}(x) = \Delta A_{\text{pore,LJ}}(x)$ . The pore Lennard-Jones contribution,  $\Delta A_{\text{pore,LJ}}$ , is nearly identical to that for the hydrophilic pore. The key difference then is the lack of Coulombic interactions which, in the hydrophilic pore, favored a particular location for the solute at the pore surface. The absence of these contributions in the hydrophobic pore leads to a minimum in  $\Delta A_{\text{pore}}(x)$  on the left-hand side instead, due to the Lennard-Jones interactions. Moreover, it gives a weaker dependence on the solute dipole moment. It is interesting to note, however, that the dependence of  $\Delta A_{\text{solv}}(x)$  on the solute dipole still gives different position distributions for the 5, 10, and 15 D solutes.

**3.3. Position-Dependent Fluorescence Spectra.** The three solutes considered in this work can be used to examine how the solute fluorescence spectrum changes upon confinement of the solvent and varies with the solute position. For this purpose, the 5 D (10 D) solute is used to represent the solute ground (excited) state. Here, we focus only on the fluorescence spectral peak positions for the three cuts across the hydrophilic pore and the  $z = 0$  Å cut across the hydrophobic pore. The full fluorescence (and absorption) spectra are provided in the Supporting Information along with tabulated spectral positions and confinement-induced shifts.

The mean peak position for the solute fluorescence along a given cut across the pore,

$$\langle \Delta E_{\text{fl}} \rangle(x) = \int \Delta E I_{\text{fl}}(\Delta E; x) d\Delta E \quad (8)$$

is plotted as a function of position,  $x$ , in Figure 6. The results show that  $\langle \Delta E_{\text{fl}} \rangle$  is nearly constant for solutes in the pore

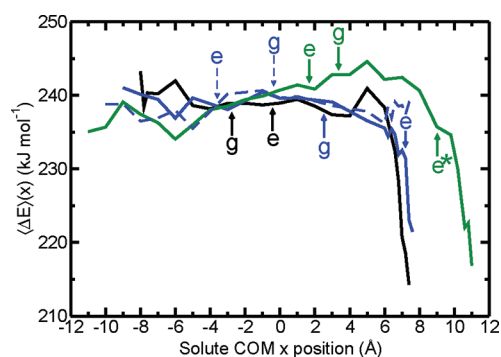


**Figure 6.** Mean spectral energy as a function of solute position in the hydrophilic pore for the cuts  $z = -10$  (black), 0 (blue), and  $+10$  Å (green) and hydrophobic pore (dashed) for  $z = 0$  (blue). The colored arrows indicate global minima in the corresponding 5 D (g) and 10 D (e) free energy curves (Figures 2 and 3), and  $e^*$  identifies the position of the interfacial peak associated with the 10 D solute in the  $z = +10$  Å cut.

interior, but changes significantly as it approaches the pore wall on the right-hand side ( $x > 0$ ) in the hydrophilic pore. This is true for all three cuts across the pore,  $z = 0$ ,  $+10$ , and  $-10$  Å. In contrast,  $\langle \Delta E_{\text{fl}} \rangle$  is effectively independent of position in the hydrophobic pore. Thus, solute diffusion from the interior to near the pore wall on the right-hand side would lead to significant shifts in the fluorescence energy in the hydrophilic pore, but only as the solute closely approaches the silica surface.

That this is an electrostatic effect is evident from the absence of this effect in the hydrophobic pore. Moreover, the fact that the fluorescence shifts occur on the right-hand side of the pore in all three cases suggests that an asymmetry in the pore structure is present. It is interesting that while this is manifested in the fluorescence, it is not observed with the same consistency in the free energy profiles.

To place the results for  $\langle \Delta E_{\text{fl}} \rangle(x)$  into the context of TDF measurements, the locations of the maxima in the solute probability distributions are indicated in Figure 6 for the ground (5 D) and excited (10 D) states. For solute diffusion to affect the TDF signal, the fluorescence energy must change as the solute shifts from the ground-state position distribution to the excited-state distribution. In the simplest analysis, the locations indicated by g and e must have different fluorescence energies. It is clear from Figure 6 that this is not the case for the  $z = -10$  Å cut. Recall that for  $z = -10$  Å the 10 D position distribution, Figure 3b, while different from the 5 D distribution, is not localized at the pore surface where the fluorescence shifts occur. In contrast, the  $z = 0$  and  $+10$  Å cuts have a position distribution with a global and local maximum, respectively, at the pore interface where the mean fluorescence energy is shifted. Thus, this shift in fluorescence energy contributes to the total spectrum for the 10 D solute at equilibrium. It is interesting to note then that different regions of the pore influence the fluorescence spectrum differently, an effect due to the pore heterogeneity that may be difficult to capture experimentally.

## 4. DISCUSSION

### 4.1. Solute Diffusion and TDF in Nanoscale Silica Pores.

As noted in section 1, for solute diffusion to contribute to emergent time scales in TDF experiments,<sup>76,74,111</sup> the system must satisfy three requirements.<sup>52</sup> (1) The solute must show a state-dependent position bias within the confining framework. (2) The fluorescence properties of the solute must change with the solute position in the confining framework and with a measurable amplitude. Requirement 1 implies that, upon excitation, the solute is in a nonequilibrium position in addition to the standard nonequilibrium solvation state, while requirement 2 is the condition for observing the subsequent diffusion through the solute fluorescence. Finally, (3) for the solute motion to be observed in a TDF measurement, the resulting contribution to the TDF signal must occur on an experimentally accessible time scale. Note that all three of these requirements have implications beyond the interpretation of TDF experiments. However, requirement 1 is particularly general and important for understanding chemistry (relevant to, for example, catalysis, separations, and sensing) independent of 2 and 3, which speak more to the observation of solute diffusion in TDF measurements.

In this work, MD simulations show that, for a model solute dissolved in ethanol confined in a silica pore, requirement 1 is met in both a hydrophilic and hydrophobic pore. While in the clearest case ( $z = 0$  Å) a distinct transition from a delocalized to localized position distribution is observed between the ground state (5 D) and excited state (10 or 15 D) of the solute, all cuts we have examined have a dependence of the distribution on the solute dipole moment. Indeed, we expect that this is a general feature in nanoconfined solvent systems. Solutes with different charge distributions will not have the same position distributions due to the differences in both pore–solute interactions at the interface and solvent–solute interactions,

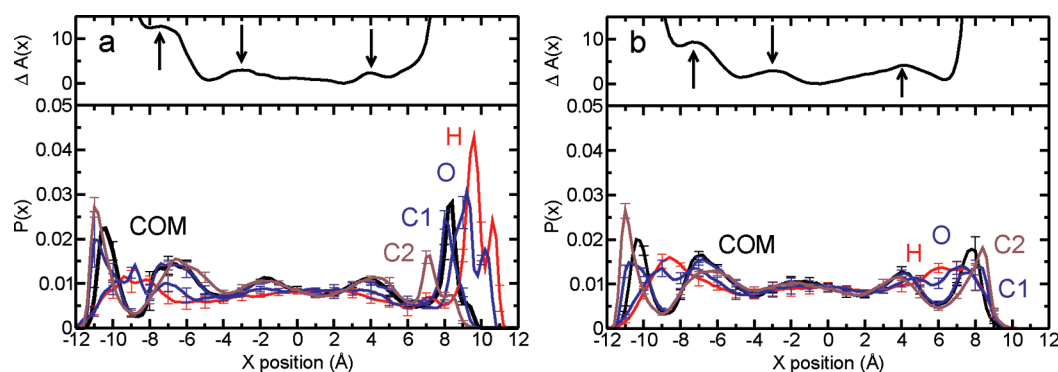


**Figure 7.** Solvent density profiles (bottom panels) in (a) hydrophilic and (b) hydrophobic pores for the ethanol center of mass (COM, black), hydrogen (H, red), oxygen (O, blue), methylene (C1, purple), and methyl (C2, brown) sites. The corresponding solute total free energy profiles (top panels), with local maxima indicated by arrows, have been included for comparison.

e.g., due to location-dependent solvent polarity. In other words, the position dependence of the Hamiltonian is modified when the solute charge distribution is changed. Naturally, the magnitude of the differences in chromophore location between the ground and excited states will depend on the solute and confining framework properties, as will any manifestation in a TDF measurement.

In particular, the present simulations find that requirement 2 is met only in the case of a hydrophilic pore and only for solute locations approaching the pore surface on one side. Thus, the model used in this work suggests that for some systems (hydrophobic pores in this case) TDF measurements will be blind to any difference in state-dependent chromophore position distributions. This indicates the need for alternative, complementary experimental probes of nanoconfined solvent systems. Finally, we note that while requirement 3 has not been addressed in this work, it must also be evaluated to fully understand the role of solute diffusion in the TDF signal,  $S(t)$ . Nonequilibrium MD simulations to evaluate the relevant time scales are currently underway.

**4.2. Relation to Previous Work.** Previous theoretical investigations have also found state-dependent positions and position-dependent fluorescence spectra, requirements 1 and 2, respectively. The key differences with the present study are the solute size, confining framework chemistry, and pore roughness. A Monte Carlo study using a smooth, spherical confining surface and a small dye model dissolved in methyl iodide or acetonitrile found that the ground-state solute preferentially resides at the interface while the most likely position for the excited-state solute is the pore interior.<sup>75</sup> Subsequent nonequilibrium MD simulations of  $S(t)$  for the same system found a contribution of solute diffusion to the solvation dynamics resulting from this difference in ground- and excited-state equilibrium positions.<sup>76</sup> These position biases are reversed from those found in this work, in which the excitation of the solute drives it to the pore interface. The difference is likely attributable to the favorable solute–pore interactions, absent in the previous study, and the solute size, which allows the present model to span several layers of varying solvent polarity. Additionally, the simple nature of the confining frameworks used in this earlier work<sup>75,76,96</sup> eliminated any effects of surface roughness and chemistry.

A state-dependent solute position was also observed in MD simulations of reverse micelles (RM).<sup>111</sup> Using  $I_2^+$  and  $I_2^-$  models of solute “excited states” of  $I_2$ , Faeder and Ladanyi showed that each excited state exhibited a distinct location

preference within the RM, which they used to explain differences in the nonequilibrium behavior of the two excited-state models.<sup>111</sup>

Recently, Elola et al. simulated the fluorescent dye coumarin 153 (C153) dissolved in methanol confined within nanoscale silica pores like those used here.<sup>79</sup> They carried out 20 ns ground-state equilibrium simulations in both hydrophilic and hydrophobic pores and found, for the most part, localization of the dye at the pore interface. In 30 ps nonequilibrium trajectories in the excited state initiated from equilibrium ground-state configurations, they found no diffusion of the C153 dye molecule. Together, their results support the notion that deep free energy minima can function as sinks for the solute molecule and that barriers to diffusion with respect to the pore interface can be large. Their results do not support a role for solute diffusion in TDF measurements in nanoscale silica pores; it is important to note, however, that experiments find solvation time scales of  $\sim 100$  ps for C153 in ethanol confined in 2.5 nm silica pores<sup>65</sup> and  $\sim 300$  ps for 3.1 nm pores.<sup>66</sup> The present thermodynamic integration approach along multiple cuts within the pore allows us to partly overcome the sampling limitations of comparatively short MD simulations; our results suggest that such free energy sinks exist at multiple locations within the pore and ground- and excited-state solutes occupy different positions in the pore. The difficulty in obtaining adequate statistical sampling is illustrated by the 150–200 ns total simulation time required here to obtain each one-dimensional free energy curve, for a simplified solute, with global minima resolved within statistical errors. Our group is actively pursuing enhanced sampling and longer NEMD trajectories, which appear necessary for adequate description of the dynamics in these systems.

The model used in the present work allows insight into the effect of varying properties of the confining framework and solute. In particular, the effect of changing the pore surface from hydrophilic to hydrophobic is significant. However, it is also interesting to note that, in the hydrophilic pore, a dramatic change in the solute position distribution, from delocalized to localized, can occur when the solute dipole is increased from 5 to 10 D, which is particularly evident for the  $z = 0$  Å cut across the pore. The implication is that the role of solute diffusion in TDF experiments may depend on both the solute proximity to specific locations on the pore surface at the time of excitation, as well as the ground-state and excited-state dipole moments of the dye, not merely the magnitude or sign of the difference in dipole moments,  $\Delta\mu = \mu_e - \mu_g$ . For example, a dye molecule



with a comparatively large,  $\sim 10$  D, ground-state dipole moment may already be localized near a specific region of the pore interface. It would not be expected to experience significant diffusion after excitation, even with a sizable change in dipole moment, e.g., from 10 to 15 D. In addition, the degree to which solute diffusion after excitation is driven by a free energy gradient, i.e., the time scale involved in condition 3, will depend upon the difference in the ground- and excited-state solute position distributions (Figure 2) and thus  $\Delta\mu$ . We note that the present model cannot speak to issues of specific solute–pore interactions such as hydrogen bonding, which may also influence the solute position and orientation, may be state-dependent, and may affect the fluorescence spectra. These effects also are currently being investigated in our laboratory using atomistic dye models.

**4.3. Influence of Solvent Structure on the Solute Position.** Previous studies of smaller solutes confined in hydrophobic cavities have found free energy profiles that are well-correlated with solvent layering.<sup>75,96</sup> Thus, the solvent structure was examined to explain the small undulations and shoulders in the solute free energy profiles in this study. Accordingly, the distribution of solvent atoms along  $x$  for the  $z = 0$  Å cut was calculated within a  $4$  Å  $\times$   $4$  Å box in the  $y$ – $z$  plane; the 5 D solute was positioned along  $z = +10$  Å to avoid perturbation of the solvent at  $z = 0$  Å. The results of this calculation are shown in Figure 7, and the corresponding total solvent contribution to the solute free energy profiles are included in the top panels for comparison. The solvent COM density profile in the hydrophilic pore shows peaks spaced by  $\sim 4$ – $5$  Å. By comparison, the undulations in the solvent contribution to the solute free energy yields a spacing of  $\sim 3.5$ – $4$  Å. This rough correspondence suggests that the undulations in the free energy are associated with the solvent layering. The same argument can be made for the hydrophobic case, in which the spacing in the solvent density is  $\sim 4$ – $5$  Å and in the free energy  $\sim 3$ – $5$  Å. While these data are suggestive, they are not conclusive. However, the increased solvent density at the pore interface in both the hydrophilic (a) and hydrophobic (b) pore correlates well with the shoulders in the solute–solvent free energy decomposition (Figures 4a and 5a). Thus, the shoulders in the solute–solvent contribution to the free energy near the pore interface can be viewed as the energy required to displace the strongly associated solvent molecules there.

Several factors may contribute to the weaker correspondence between solvent layering and free energy seen here compared to previous reports. In those studies, the solute models were comparable in size to the solvent, leading to solutes lying within a solvent layer or spanning across two layers.<sup>75,76,96</sup> Here, the influence of the solvent on the solute free energy is complicated by the fact that the solute spans several solvent layers of differing effective polarity. In addition, the heterogeneous chemistry (placement of silanol groups) and roughness of the pore surface also influence the solvent layering, as discussed below. Finally, the correlation between solvent layering and solute free energy appears to be stronger for linear solvents (e.g.,  $\text{CH}_3\text{I}$ ,  $\text{CH}_3\text{CN}$ ) than for nonlinear solvents like methanol or ethanol,<sup>96</sup> presumably due to packing effects.

**4.4. Influence of Pore Interactions on the Solute Position.** It is apparent from the solvent density profiles shown in Figure 7a that the two sides of the pore are significantly different, a general feature evidenced in the free energy profiles, Figures 2 and 3. On the left-hand side ( $x < 0$ ) of the hydrophilic pore (Figure 7a), the ethanol solvent methylene

and methyl groups reside at the pore interface while the oxygen and hydrogen point toward the pore interior, similar to the solvent organization within the hydrophobic pore (Figure 7b). However, the right-hand side ( $x > 0$ ) of the pore shows the hydrogen closest to the interface, with oxygen, methylene, and methyl sites increasingly distant from the interface. This strong ordering in the solvent density profile, indicative of ethanol hydrogen bonding with the pore surface, occurs at the same location where the 10 and 15 D solutes exhibit a strong free energy minimum. Indeed, in this region of the pore are several silanol groups. These results are consistent with the conclusion that the free energy minimum for the 10 and 15 D solutes in the hydrophilic pore for  $z = 0$  Å is determined by solute–pore interactions (see section 3.2). When those interactions are absent, as on the left-hand side of the pore or in the hydrophobic pore, no minimum is observed. The degree to which the surface chemistry gives rise to free energy minima can be seen by considering the other cuts across the pore. The small free energy minimum on the right side ( $x > 0$ ) of the pore along the  $z = +10$  Å cut occurs where the solute can contact a single silanol group there. No silanol groups are found on the left side of the pore. Similarly, for the  $z = -10$  Å cut, no silanol groups are present at the surface on either side. The role of specific functional groups and surface topology in determining the solute free energy as a function of position in the pore sites is currently under investigation. In any case, preliminary results from unconstrained MD simulations suggest that it is reasonable to think that the heterogeneity observed in the present work is representative of the environments experienced by the solute in the full pore.

## 5. SUMMARY

Molecular dynamics simulations of a model solute dissolved in ethanol and confined in a silica pore have been used to investigate the position-dependence of the free energy and electronic spectra along one-dimensional cuts across the width of the pore. The effect of the solute dipole moment and pore surface interactions have also been investigated. The results indicate that the solute position can change dramatically, e.g., from delocalized to localized, as the dipole moment is varied. At the same time, the solute position distribution differs between hydrophilic and hydrophobic silica pores, an effect attributable to the solute–pore Coulombic interactions. These electrostatic contributions are also responsible for shifts in the solute fluorescence spectrum as it approaches some locations on the hydrophilic wall, an effect absent in the hydrophobic pore.

In the context of time-dependent fluorescence measurements on nanoconfined solvent systems, the results provide insight into the potential contribution of solute diffusion to the TDF signal. Specifically, in both hydrophilic and hydrophobic silica pores, the position distribution of the solute depends on its dipole moment, which effectively represents the electronic state for dyes with charge-transfer transitions. Such a state-dependent solute position is requirement 1 for solute diffusion to contribute to the emergence of new time scales in TDF experiments, as discussed in section 1. In contrast, the fluorescence spectrum for a solute in the hydrophobic pore is effectively independent of position, while it changes sharply near one pore surface in the hydrophilic case. A change in the fluorescence spectrum with solute position is requirement 2 for a solute diffusion contribution to the TDF signal (section 1). This is clearly not met in the case of the hydrophobic (uncharged) pore surface, but it is for the hydrophilic silica



pore. This difference suggests how TDF measurements may be specific to the precise system studied, a conclusion that is also supported by the qualitative and quantitative variations in reported results for nanoconfined solvents. A third requirement remains, which is that the solute diffusion occurs on a time scale observable in an experiment. This is currently being studied in our group for both the model solute used in this work and atomistic models of dye molecules.

It is useful to consider what the present results suggest about chemistry more generally in nanoconfined solvents. The finding that the position distribution for a solute depends on its charge distribution, consistent with previous studies in simpler nanocavities,<sup>49,50,75,76,96,111</sup> suggests routes for tunability of mesoporous materials. In particular, the solute position distribution is found to depend on both the solute dipole moment and the confining framework properties such as local structure and overall hydrophilicity. It should be possible to exploit these dependencies to design materials for specific applications. On the other hand, the sensitivity of the solute position distributions and fluorescence spectra to the solute and framework properties indicates why there is still no unified picture of TDF and, more generally, chemistry in nanoconfined solvents.<sup>52</sup> Further work will be required in which simulations and experiments can be directly compared for specific, well-characterized systems, combined with an exploration of the effects of varying solute and confining framework properties.

Finally, it is interesting to note that while the solute position distributions depend on the solute dipole moment in both hydrophilic pores and hydrophobic pores, the fluorescence spectra are only sensitive to the dye position in the former case. Thus, for the hydrophobic pore system considered here, a TDF experiment would be unable to observe the solute diffusion after excitation predicted to occur. Yet, the state-dependent position of the solute might still have significant importance in applications of porous materials. This is an important reminder that measurements only reflect properties to which they are sensitive, and should be interpreted carefully for nanoconfined solvents.<sup>31,35</sup> Our understanding of dynamics in nanoconfined solvents is still developing and will require both better models and the development of new experimental probes.

The model solute dye used here provides an opportunity to examine general effects of nanoconfinement on solvation properties. Specifically, effects of solute size and dipole moment can be examined independently of specific dye–pore or dye–solvent interactions that may be present for a realistic dye molecule. In this sense, such models complement simulations involving atomistic representations of dye molecules. Given the lack of a single, universal result for how the TDF signal changes upon confinement, both types of studies will be required to uncover both the important, general features of nanoconfined solvation dynamics and the effects specific to a particular system.

## ■ ASSOCIATED CONTENT

### Supporting Information

Potential parameters, radial distribution functions, and calculated spectra. This material is available free of charge via the Internet at <http://pubs.acs.org>.

## ■ AUTHOR INFORMATION

### Corresponding Author

\*E-mail: [wthompson@ku.edu](mailto:wthompson@ku.edu).

## Notes

The authors declare no competing financial interest.

## ■ ACKNOWLEDGMENTS

W.H.T. acknowledges support for this work from the Chemical Sciences, Geosciences, and Biosciences Division, Office of Basic Energy Sciences, Office of Science, U.S. Department of Energy.

## ■ REFERENCES

- (1) Dorazio, F.; Bhattacharja, S.; Halperin, W. P.; Eguchi, K.; Mizusaki, T. *Phys. Rev. B* **1990**, *42*, 9810–9818.
- (2) Korb, J. P.; Xu, S.; Jonas, J. J. *Chem. Phys.* **1993**, *98*, 2411–2422.
- (3) Koone, N.; Shao, Y.; Zerda, T. W. *J. Phys. Chem.* **1995**, *99*, 16976–16981.
- (4) Harpham, M. R.; Ladanyi, B. M.; Levinger, N. E.; Herwig, K. W. *J. Chem. Phys.* **2004**, *121*, 7855–7868.
- (5) Nikiel, L.; Hopkins, B.; Zerda, T. W. *J. Phys. Chem.* **1990**, *94*, 7458–7464.
- (6) Liu, G.; Li, Y.-Z.; Jonas, J. J. *Chem. Phys.* **1989**, *90*, 5881–5882.
- (7) Liu, G.; Li, Y.-Z.; Jonas, J. J. *Chem. Phys.* **1991**, *95*, 6892–6901.
- (8) Liu, G.; Mackowiak, M.; Li, Y.-Z.; Jonas, J. J. *Chem. Phys.* **1991**, *94*, 239–242.
- (9) Zhang, J.; Jonas, J. J. *Phys. Chem.* **1993**, *97*, 8812–8815.
- (10) Xu, S.; Kim, Y. J.; Jonas, J. *Chem. Phys. Lett.* **1994**, *218*, 329–332.
- (11) Korb, J. P.; Delville, A.; Xu, S.; Demeulenaere, G.; Costa, P.; Jonas, J. J. *Chem. Phys.* **1994**, *101*, 7074–7081.
- (12) Wallen, S. L.; Nikiel, L.; Yi, J.; Jonas, J. J. *Phys. Chem.* **1995**, *99*, 15421–15427.
- (13) Yi, J.; Jonas, J. J. *Phys. Chem.* **1996**, *100*, 16789–16793.
- (14) Korb, J. P.; Malier, L.; Cros, F.; Xu, S.; Jonas, J. *Phys. Rev. Lett.* **1996**, *77*, 2312–2315.
- (15) Korb, J. P.; Xu, S.; Cros, F.; Malier, L.; Jonas, J. J. *Chem. Phys.* **1997**, *107*, 4044–4050.
- (16) Farrer, R. A.; Loughnane, B. J.; Fourkas, J. T. *J. Phys. Chem. A* **1997**, *101*, 4005–4010.
- (17) Loughnane, B. J.; Fourkas, J. T. *J. Phys. Chem. B* **1998**, *102*, 10288–10294.
- (18) Loughnane, B. J.; Farrer, R. A.; Fourkas, J. T. *J. Phys. Chem. B* **1998**, *102*, 5409–5412.
- (19) Loughnane, B. J.; Farrer, R. A.; Scodinu, A.; Fourkas, J. T. *J. Chem. Phys.* **1999**, *111*, 5116–5123.
- (20) Loughnane, B. J.; Farrer, R. A.; Scodinu, A.; Reilly, T.; Fourkas, J. T. *J. Phys. Chem. B* **2000**, *104*, 5421–5429.
- (21) Scodinu, A.; Farrer, R. A.; Fourkas, J. T. *J. Phys. Chem. B* **2002**, *106*, 12863–12865.
- (22) Scodinu, A.; Fourkas, J. T. *J. Phys. Chem. B* **2002**, *106*, 10292–10295.
- (23) Farrer, R. A.; Fourkas, J. T. *Acc. Chem. Res.* **2003**, *36*, 605–612.
- (24) Zhu, X.; Farrer, R. A.; Fourkas, J. T. *J. Phys. Chem. B* **2005**, *109*, 12724–12730.
- (25) Faeder, J.; Albert, M. V.; Ladanyi, B. M. *Langmuir* **2003**, *19*, 2514–2520.
- (26) Tan, H.-S.; Piletic, I. R.; Riter, R. E.; Levinger, N. E.; Fayer, M. D. *Phys. Rev. Lett.* **2005**, *94*, 057405.
- (27) Piletic, I. R.; Moilanen, D. E.; Spry, D. B.; Levinger, N. E.; Fayer, M. D. *J. Phys. Chem. A* **2006**, *110*, 4985–4999.
- (28) Moilanen, D. E.; Levinger, N. E.; Spry, D. B.; Fayer, M. D. *J. Am. Chem. Soc.* **2007**, *129*, 14311–14318.
- (29) Fayer, M. D.; Levinger, N. E. *Annu. Rev. Anal. Chem.* **2010**, *3*, 89–107.
- (30) Pieniazek, P. A.; Lin, Y.-S.; Chowdhary, J.; Ladanyi, B. M.; Skinner, J. L. *J. Phys. Chem. B* **2009**, *113*, 15017–15028.
- (31) Morales, C. M.; Thompson, W. H. *J. Phys. Chem. A* **2009**, *113*, 1922–1933.
- (32) Laage, D.; Thompson, W. H. *J. Chem. Phys.* **2011**, submitted.
- (33) Luo, R. S.; Jonas, J. J. *Raman Spectrosc.* **2001**, *32*, 975–978.

- (34) Gomez, J. A.; Tucker, A. K.; Shepherd, T. D.; Thompson, W. H. *J. Phys. Chem. B* **2005**, *109*, 17479–17487.
- (35) Gulmen, T. S.; Thompson, W. H. *Langmuir* **2006**, *22*, 10919–10923.
- (36) Das, S.; Datta, A.; Bhattacharyya, K. *J. Phys. Chem. A* **1997**, *101*, 3299–3304.
- (37) Mandal, D.; Pal, S. K.; Bhattacharyya, K. *J. Phys. Chem. A* **1998**, *102*, 9710–9714.
- (38) Kwon, O.-H.; Jang, D.-J. *J. Phys. Chem. B* **2005**, *109*, 8049–8052.
- (39) Kwon, O.-H.; Jang, D.-J. *J. Phys. Chem. B* **2005**, *109*, 20479–20484.
- (40) Kwon, O.-H.; Kim, T. G.; Lee, Y.-S.; Jang, D.-J. *J. Phys. Chem. B* **2006**, *110*, 11997–12004.
- (41) Lee, Y.-S.; Kwon, O.-H.; Jang, D.-J. *Phys. Chem. Chem. Phys.* **2008**, *10*, 153–158.
- (42) Park, S.-Y.; Kwon, O.-H.; Kim, T. G.; Jang, D.-J. *J. Phys. Chem. C* **2009**, *113*, 16110–16115.
- (43) Garcia-Ochoa, I.; Lopez, M. A. D.; Vinas, M. H.; Santos, L.; Ataz, E. M.; Amat-Guerri, F.; Douhal, A. *Chem.—Eur. J.* **1999**, *5*, 897–901.
- (44) Angulo, G.; Organero, J. Á.; Carranza, M. A.; Douhal, A. *J. Phys. Chem. B* **2006**, *110*, 24231–24237.
- (45) Douhal, A.; Angulo, G.; Gil, M.; Organero, J. A.; Sanz, M.; Tormo, L. *J. Phys. Chem. B* **2007**, *111*, 5487–5493.
- (46) Gil, M.; Wang, S.; Organero, J. A.; Teruel, L.; Garcia, H.; Douhal, A. *J. Phys. Chem. C* **2009**, *113*, 11614–11622.
- (47) Cohen, B.; Wang, S.; Organero, J. A.; Campo, L. F.; Sanchez, F.; Douhal, A. *J. Phys. Chem. C* **2010**, *114*, 6281–6289.
- (48) Gil, M.; Martin, C.; Organero, J. A.; Navarro, M. T.; Corma, A.; Douhal, A. *J. Phys. Chem. C* **2010**, *114*, 6311–6317.
- (49) Thompson, W. H. *J. Phys. Chem. B* **2005**, *109*, 18201–18208.
- (50) Li, S.; Thompson, W. H. *J. Phys. Chem. B* **2005**, *109*, 4941–4946.
- (51) Mitchell-Koch, K. R.; Thompson, W. H. *J. Phys. Chem. B* **2008**, *112*, 7448–7459.
- (52) Thompson, W. H. *Annu. Rev. Phys. Chem.* **2011**, *62*, 599–619.
- (53) Riter, R. E.; Undiks, E. P.; Kimmel, J. R.; Levinger, N. E. *J. Phys. Chem. B* **1998**, *102*, 7931–7938.
- (54) Willard, D. M.; Riter, R. E.; Levinger, N. E. *J. Am. Chem. Soc.* **1998**, *120*, 4151–4160.
- (55) Pant, D.; Riter, R. E.; Levinger, N. E. *J. Chem. Phys.* **1998**, *109*, 9995–10003.
- (56) Riter, R. E.; Willard, D. M.; Levinger, N. E. *J. Phys. Chem. B* **1998**, *102*, 2705–2714.
- (57) Riter, R. E.; Undiks, E. P.; Levinger, N. E. *J. Am. Chem. Soc.* **1998**, *120*, 6062–6067.
- (58) Pant, D.; Levinger, N. E. *Langmuir* **2000**, *16*, 10123–10130.
- (59) Willard, D. M.; Levinger, N. E. *J. Phys. Chem. B* **2000**, *104*, 11075–11080.
- (60) Corbeil, E. M.; Levinger, N. E. *Langmuir* **2003**, *19*, 7264–7270.
- (61) Corbeil, E. M.; Riter, R. E.; Levinger, N. E. *J. Phys. Chem. B* **2004**, *108*, 10777–10784.
- (62) Faeder, J.; Ladanyi, B. M. *J. Phys. Chem. B* **2001**, *105*, 11148–11158.
- (63) Faeder, J.; Ladanyi, B. M. *J. Phys. Chem. B* **2005**, *109*, 6732–6740.
- (64) Baumann, R.; Ferrante, C.; Deeg, F. W.; Bräuchle, C. *J. Chem. Phys.* **2001**, *114*, 5781.
- (65) Baumann, R.; Ferrante, C.; Kneuper, E.; Deeg, F. W.; Brauchle, C. *J. Phys. Chem. A* **2003**, *107*, 2422–2430.
- (66) Kamijo, T.; Yamaguchi, A.; Suzuki, S.; Teramae, N.; Itoh, T.; Ikeda, T. *J. Phys. Chem. A* **2008**, *112*, 11535–11542.
- (67) Kometani, N.; Hoshihara, Y.; Yonezawa, Y.; Kajimoto, O.; Hara, K.; Ito, N. *J. Phys. Chem. A* **2004**, *108*, 9479–9483.
- (68) Sarkar, N.; Das, K.; Datta, A.; Das, S.; Bhattacharyya, K. *J. Phys. Chem.* **1996**, *100*, 10523–10527.
- (69) Pal, S. K.; Sukul, D.; Mandal, D.; Sen, S.; Bhattacharyya, K. *J. Phys. Chem. B* **2000**, *104*, 2613–2616.
- (70) Nandi, N.; Bhattacharyya, K.; Bagchi, B. *Chem. Rev.* **2000**, *100*, 2013–2045.
- (71) Bhattacharyya, K.; Bagchi, B. *J. Phys. Chem. A* **2000**, *104*, 10603–10613.
- (72) Dutta, P.; Sen, P.; Mukherjee, S.; Halder, A.; Bhattacharyya, K. *J. Phys. Chem. B* **2003**, *107*, 10815–10822.
- (73) Bhattacharyya, K. *Acc. Chem. Res.* **2003**, *36*, 95–101.
- (74) Bhattacharyya, K.; Bagchi, B. *J. Chem. Sci.* **2007**, *119*, 113–121.
- (75) Thompson, W. H. *J. Chem. Phys.* **2002**, *117*, 6618–6628.
- (76) Thompson, W. H. *J. Chem. Phys.* **2004**, *120*, 8125.
- (77) Feng, X.; Thompson, W. H. *J. Phys. Chem. C* **2007**, *111*, 18060–18072.
- (78) Feng, X.; Thompson, W. H. *J. Phys. Chem. C* **2010**, *114*, 4279–4290.
- (79) Elola, M. D.; Rodriguez, J.; Laria, D. *J. Phys. Chem. B* **2011**, *115*, 12859–12867.
- (80) Zhang, J.; Bright, F. V. *J. Phys. Chem.* **1991**, *95*, 7900–7907.
- (81) Shiota, H.; Horie, K. *J. Phys. Chem. B* **1999**, *103*, 1437–1443.
- (82) Shiota, H.; Segawa, H. *Langmuir* **2004**, *20*, 329–335.
- (83) Riter, R. E.; Undiks, E. P.; Kimmel, J. R.; Levinger, N. E. *J. Phys. Chem. B* **1998**, *102*, 7931–7938.
- (84) Willard, D. M.; Riter, R. E.; Levinger, N. E. *J. Am. Chem. Soc.* **1998**, *120*, 4151–4160.
- (85) Willard, D. M.; Levinger, N. E. *J. Phys. Chem. B* **2000**, *104*, 11075–11080.
- (86) Pant, D.; Riter, R. E.; Levinger, N. E. *J. Chem. Phys.* **1998**, *109*, 9995.
- (87) Corbeil, E. M.; Levinger, N. E. *Langmuir* **2003**, *19*, 7264–7270.
- (88) Corbeil, E. M.; Riter, R. E.; Levinger, N. E. *J. Phys. Chem. B* **2004**, *108*, 10777–10784.
- (89) Hazra, P.; Chakrabarty, D.; Sarkar, N. *Chem. Phys. Lett.* **2003**, *371*, 553–562.
- (90) Mitra, R. K.; Sinha, S. S.; Pal, S. K. *Langmuir* **2008**, *24*, 49–56.
- (91) Chakraborty, A.; Seth, D.; Setua, P.; Sarkar, N. *J. Phys. Chem. B* **2006**, *110*, 5359–5366.
- (92) Czeslik, C.; Kim, Y. J.; Jonas, J. *J. Raman Spectrosc.* **2000**, *31*, 571–575.
- (93) Venables, D. S.; Huang, K.; Schmuttenmaer, C. A. *J. Phys. Chem. B* **2001**, *105*, 9132–9138.
- (94) Moilanen, D. E.; Fenn, E. E.; Wong, D. B.; Fayer, M. D. *J. Am. Chem. Soc.* **2009**, *131*, 8318–8328.
- (95) Moilanen, D. E.; Fenn, E. E.; Wong, D. B.; Fayer, M. D. *J. Chem. Phys.* **2009**, *131*, 014704.
- (96) Mitchell-Koch, K. R.; Thompson, W. H. *J. Phys. Chem. C* **2007**, *111*, 11991–12001.
- (97) Gomez, J. A.; Thompson, W. H. *J. Phys. Chem. B* **2004**, *108*, 20144–20154.
- (98) Kometani, N.; Arzhantsev, S.; Maroncelli, M. *J. Phys. Chem. A* **2006**, *110*, 3405–3413.
- (99) Jorgensen, W. L. *J. Phys. Chem.* **1986**, *90*, 1276–1284.
- (100) Jorgensen, W. L.; Madura, J. D.; Swenson, C. J. *J. Am. Chem. Soc.* **1984**, *106*, 6638–6646.
- (101) Gulmen, T. S.; Thompson, W. H. *Dynamics in Small Confining Systems VIII*; Fourkas, J.T., Levitz, P., Overney, R., Urbakh, M., Eds.; Materials Research Society Symposium Proceedings 899E; Materials Research Society: Warrendale, PA, 2005.
- (102) Brodka, A.; Zerda, T. W. *J. Chem. Phys.* **1996**, *104*, 6319–6326.
- (103) The DL\_POLY Molecular Simulation Package, [http://www.ccp5.ac.uk/DL\\_POLY](http://www.ccp5.ac.uk/DL_POLY).
- (104) Nosé, S. *Mol. Phys.* **1984**, *52*, 255–268.
- (105) Hoover, W. G. *Phys. Rev. A* **1985**, *31*, 1695–1697.
- (106) Fennell, C. J.; Gezelter, J. D. *J. Chem. Phys.* **2006**, *124*, 234104.
- (107) Furse, K. E.; Corcelli, S. A. *J. Chem. Theory Comput.* **2009**, *9*, 1959–1967.
- (108) The damped shifted force approach was tested by calculating the forces on the solute required for the thermodynamic integration at two solute positions, one near the pore wall and one in the interior. In both cases the forces were the same within statistical errors as those obtained using an Ewald sum.

(109) Shoemaker, D. P.; Garland, C. W.; Nibler, J. W. *Experiments in Physical Chemistry*; McGraw-Hill: New York, 1989.

(110) This is in good agreement with a grand canonical Monte Carlo simulation which gives  $126 \pm 2$  ethanol molecules in the same pore with no solute.

(111) Faeder, J.; Ladanyi, B. M. *J. Phys. Chem. B* **2001**, *105*, 11148–11158.